Supporting Information

Monolith floatable dual-function solar photothermal evaporator: Efficient cleanwater regeneration synergizing with pollutant degradation

Hongyao Zhao [a], Danhong Shang [a], Haodong Li [a], Marliyana Aizudin [b], Hongyang Zhu [a], Xiu Zhong [a], Yang Liu [a], Zhenxiao Wang [a], Ruiting Ni [a], Yanyun Wang [a], Sheng Tang [a], Edison Huixiang Ang [b,*], Fu Yang[a,*]

a School of Environmental and Chemical Engineering, Jiangsu University of Science and Technology, Zhenjiang 212003, Jiangsu, China

b Natural Sciences and Science Education, National Institute of Education, Nanyang Technological University, Singapore 637616, Singapore.

* Corresponding authors.

email addresses: fuyang@just.edu.cn; (F. Yang), edison.ang@nie.edu.sg (E. H. Ang).

1. Materials and Methods

1.1 Materials and chemicals

Copper (II) acetylpyruvate ($C_{10}H_{14}CuO_4$), iron (III) acetylpyruvate ($C_{15}H_{21}FeO_6$), potassium perbisulfate complex salt (PMS), polyacrylonitrile (PAN), and N, n-dimethylformamide (DMF) were acquired from Energy Limited. Sodium chloride (NaCl) and Sodium Alginate ($(C_6H_7O_6Na)_n$) were obtained from Shanghai Aladdin Industrial Co., LTD. Methylene Blue (MB), Congo Red (CR), Rhodamine B (RB), Methyl Orange (MO), Tetracycline (TC), and Oxytetracycline (OTC) were sourced from Macklin. Various sizes of melamine porous sponges were procured from Xuxian Building Materials Co., Ltd. Hydrophilic polytetrafluoroethylene (PTFE) filter membranes were purchased from Nova Stationery flagship store. Bohai Sea Water was acquired from Bohai Liaoshen store. All chemical reagents were of analytical quality and could be used directly after delivery without the need for purification.

1.2. Fabrication of FeCu/CNF membrane

1.2.1 Synthesis of photothermal fiber

In a 10 mL DMF solution, 0.3532 g of $C_{15}H_{21}FeO_6$ (1 mmol) and 0.2618 g of $C_{10}H_{14}CuO_4$ (1 mmol) were stirred at 2000 rpm. 1 g of PAN was added and stirred for 12 h, resulting in a uniform viscous spinning solution. This solution was loaded into a 10 mL syringe and electrospun using 18 kV voltage, 0.6 mL h^{-1} injector pump rate, 350-400 rpm rotating shaft speed, and a spinning temperature of 35 °C. The membranes were dried in a vacuum oven at 60 °C for 24 h. Afterward, the product underwent pre-treatment in a muffle furnace at 200 °C, with a heating rate of 2 °C min^{-1}, followed by calcination at 700 °C in a N2 atmosphere for 2 h to yield FeCu/CNF@1 composite. The same steps were repeated using 1.5 mmol, 2 mmol, and 3 mmol of $C_{15}H_{21}FeO_6$ to produce

FeCu/CNF@1.5, FeCu/CNF@2, FeCu/CNF@3, and FeCu/CNF@4, respectively. For control, 1.4127 g of $C_{15}H_{21}FeO_6$ (4 mmol) and 1.047 g of $C_{10}H_{14}CuO_4$ (4 mmol) were added to 10 mL DMF solution. The same steps were repeated to produce metal salt carbon nanofiber, Fe/CNF, and Cu/CNF.

1.2.2 Preparation of 2D evaporator

To create the FeCu/CNF membrane, a 0.02 kg m^{-2} sample of FeCu/CNF composite was weighed and then subjected to ultrasonication with deionized (DI) water until a well-dispersed black solution was achieved. Subsequently, the homogeneous black-coloured solution was uniformly deposited onto a hydrophilic polytetrafluoroethylene (PTFE) filter membrane (2.5 cm in diameter) through vacuum filtration and left to air-dry. Then, the steps were repeated to prepare CNF, FeCu/CNF@1, FeCu/CNF@1.5, FeCu/CNF@2, FeCu/CNF@3, and FeCu/CNF@4 membrane, respectively.

1.3. Preparation of S-FeCu/CNF, D-S-FeCu/CNF evaporator

Following the inspiration mentioned earlier, the evaporator fabrication process is as follows. 40 mg of FeCu/CNF@3 was dissolved in 10 mL of deionized water with vigorous stirring at room temperature. Subsequently, 20 mg of sodium alginate (SA) was added, and continuous stirring was maintained for 1 hour to create the S-FeCu/CNF slurry. This slurry was evenly drop-cast onto melamine sponges (3.4 cm in diameter, 0.5 cm thick) and soaked in a 3 mg mL^{-1} $CaCl_2$ solution for calcium ion network crosslinking, forming a hydrogel. The resulting composite was dried overnight in a 50 °C oven. The S-FeCu/CNF-40 evaporator was then washed with DI water to remove excess impurities. Additionally, various amounts of FeCu/CNF@3 composite (10 mg, 20 mg, 30 mg, 50 mg) were used to create S-FeCu/CNF-10, S-FeCu/CNF-20, S-FeCu/CNF-30, and S-FeCu/CNF-50, respectively. For the dual-functional monolithic evaporator, the melamine sponge was directly immersed in the

above-mentioned slurry and then in the same concentration of $CaCl_2$ solution to create a hydrogel. After drying and rinsing with deionized water, the dual-functional monolithic evaporator (D-S-FeCu/CNF-40) was obtained.

1.4. Characterizations

Various analytical instruments were employed to scrutinize the surface and composition of the materials. Surface examination was conducted using a field emission scanning electron microscope (Zeiss Merlin, Germany). The elemental states of the samples were determined with an X-ray photoelectron spectrometer (ULVAC-PHI 5000, Kanagawa, Japan) equipped with monochromatic Al Kα radiation (1486.6 eV), utilizing the C1s peak at 284.6 eV as a reference for binding energy. For further analysis, a transmission electron microscope (JEM-2010) with an accelerating voltage of 200 kV was equipped for elemental mapping. The phase and element composition were identified through X-ray diffractometry (Shimadzu XRD-6000) using a Cu-Kα radiation source. Raman spectroscopy (SPEX Triplemate 1877D) with a resolution of 2 cm^{-1} was employed to detect the presence of bands, while contact angle measurements (Attension Theta Flex) assessed water wetting and absorption capabilities. Light absorption capacity across a wavelength range of 200-2500 nm was determined using a solid UV-vis spectrophotometer (Perkin Elmer lambda 750, Shimadzu UV-3600). Structural properties, including pore size distribution and specific surface area, were measured with a Belsorp vapor adsorption instrument (McBayer, Japan). To analyze the concentration of dyes, such as methyl blue (MB), in both contaminated and purified water, an ultraviolet-visible spectrometer (UV-1800) was utilized. Additionally, an inductively coupled plasma spectrometer (ICP-OES, PE-8000) was employed to measure the levels of metal cations (K^+, Ca^{2+}, Na^+, and Mg^{2+}) in the collected desalinated water.

1.5. Solar vapor generation and desalination experiment

The experimental setup included a solar simulator (Solar-500T, NBeT, Beijing, China) with a light intensity of 1 kW m^{-2} (one sun), measured using a photopower meter (FZ400, NBeT, Beijing, China). An analytical balance (BSM-320.3, Zhuojing, Shanghai, China) recorded real-time weight data. Infrared thermal images were captured using a thermal imager (UNI-T, UTi260B). The room was maintained at approximately 25 °C, with a humidity level of 40% during the tests. For indoor experiments, a FeCu/CNF membrane with a 25 mm diameter was placed on air cushion paper. A 1 cm thick polyethylene (PE) foam was supported on a beaker containing seawater from the Bohai Sea, creating a FeCu/CNF membrane solar evaporator device. Similarly, a 34 mm diameter S-FeCu/CNF evaporator was positioned on air cushion paper, and 1 cm thick polyethylene (PE) foam was supported on a beaker containing Bohai Sea seawater to create a monolithic S-FeCu/CNF solar evaporator unit. Outdoor desalination experiments evaluated the practicality of the solar evaporator chamber setup from 08:30 to 17:30 h. A transparent trapezoidal box, constructed from 3 mm thick acrylic sheets, featured a bottom surface size of 31 × 21.5 cm^2, a front height of 7.5 cm, and a rear height of 24 cm. Seawater samples were collected from the Bohai Sea, and hourly seawater mass loss data were recorded for evaporation rate calculations. Solar radiation intensity (0.7-1 kW m^{-2}), wind speed (less than or equal to 3.5 m s^{-1}), and relative humidity (30 %) were also monitored.

1.6. D-S-FeCu/CNF Catalytic degradation of MB

In AOP experiment, MB degradation was carried out in a beaker containing MB solution (20 ppm, 50 mL) and D-S-FeCu/CNF evaporator. Firstly, 50 mL MB solution was added into 100 mL beaker, and the solution was continuously stirred with a magnetic agitator (200 rpm), then PMS (0.049 mM) was added, 3

mL solution was extracted for ultraviolet spectrophotometer analysis and recorded as the initial value, and then D-S-FeCu/CNF evaporator was added. The evaporator floats on the surface of the water and projects simulated sunlight (1 kW m^{-2}), which then starts timing. Every 10 min, 3 mL solution was extracted and analyzed by ultraviolet spectrophotometer. For 50 mins, the UV absorption wavelength is 665 nm.

In the context of solar steam generation, the evaluation of thermal heat losses plays a crucial role, encompassing three key components: radiation, convection, and conduction. The following analysis provides a detailed breakdown[1-4]:

1. Radiation:

The thermal radiation losses can be quantified using the Stefan-Boltzmann equation as follows:

$$\emptyset = \varepsilon A \sigma (T_1^4 - T_2^4) \quad (1)$$

here, $\emptyset$ represents the heat flux, where ε is the emissivity (with a value of 1), A is the effective evaporation surface area (490 mm^2), σ is the Stefan-Boltzmann constant (5.67×10-8 W m^{-2} K^{-4}), T1 signifies the surface temperature of the membrane post-evaporation under solar illumination (approximately 45.1 ℃ or 318.3 K), and T2 corresponds to the ambient temperature above the film. Consequently, the thermal radiation losses were computed for FeCu/CNF@4, FeCu/CNF@3, FeCu/CNF@2, FeCu/CNF@1.5, FeCu/CNF@1, Fe/CNF, Cu/CNF, and CNF membranes, yielding values of 6.8%, 6.78%, 7.1%, 6.79%, 7.1%, 6.78%, 7.04%, and 6.7%, respectively.

2. Convection

Convective heat loss is determined by Newton's law of cooling, expressed as follows:

$Q = hA\Delta T$ (2)

Here, Q denotes the convective heat flux, where h represents the convective heat transfer coefficient (approximately 5 W m^{-2} K^{-1}), A signifies the effective evaporation surface area (about 490 mm^2), and ∆T stands for the temperature difference between the surface temperature of the prepared solar evaporation material and the ambient temperature. Consequently, the convective heat losses were computed for FeCu/CNF@4, FeCu/CNF@3, FeCu/CNF@2, FeCu/CNF@1.5, FeCu/CNF@1, Fe/CNF, Cu/CNF, and CNF membranes, yielding values of 5.49%, 5.15%, 5.44%, 5.24%, 5.51%, 5.32%, and 5.22%, respectively.

3. Conduction

Thermal conduction heat loss arises from the heat transferred from the prepared material to the water, with its calculation formula as follows:

$$q = kA\frac{(T_1 - T_2)}{L} \quad (3)$$

here, q represents the heat transfer, where k denotes the thermal conductivity of PE foam (approximately 0.042 W m^{-1} K^{-1}), A stands for the heat exchange surface area (about 490 mm^2), T1 and T2 represent the temperature difference between the surface temperature and the ambient temperature of the prepared solar evaporation material after reaching steady-state temperature, and L signifies the thickness of the PC foam support (13 mm). Consequently, the thermal conductivity and heat loss were computed for FeCu/CNF@4, FeCu/CNF@3, FeCu/CNF@2, FeCu/CNF@1.5, FeCu/CNF@1, Fe/CNF, Cu/CNF, and CNF membranes, yielding values of 2.53%, 2.37%, 2.51%, 2.42%, 2.54%, 2.45%, 2.56%, and 2.4%, respectively.

In summary, the total heat loss for the FeCu/CNF@3 membrane during water evaporation is approximately 14.3%, comprising contributions from radiation (6.78%), convection (5.15%), and conduction (2.37%). The FeCu/CNF@4 membrane exhibits a heat loss of around 14.82%, with components from radiation (6.8%), convection (5.49%), and conduction

(2.53%). The FeCu/CNF@2 membrane records a heat loss of 15.05%, encompassing radiation (7.1%), convection (5.44%), and conduction (2.51%). The FeCu/CNF@1.5 membrane demonstrates a heat loss of 14.45%, involving radiation (6.79%), convection (5.24%), and conduction (2.42%). The FeCu/CNF@1 membrane presents a heat loss of 15.15%, including radiation (7.1%), convection (5.51%), and conduction (2.54%). The Fe/CNF membrane showcases a heat loss of 14.55%, with components from radiation (6.78%), convection (5.32%), and conduction (2.45%). The Cu/CNF membrane displays a heat loss of 15.14%, comprising radiation (7.04%), convection (5.54%), and conduction (2.56%). Lastly, the 2D-CNF membrane features a heat loss of 14.32%, encompassing radiation (6.7%), convection (5.22%), and conduction (2.4%).

Table S1. An overview of the solar steam generation performance achieved by recently reported photothermal materials when exposed to one sun irradiation.

Light intensity kWm^{-2}	**Photothermal system**	**Multi-functional**	**Water evaporation rate ($kg\ m^{-2}\ h^{-1}$)**	**Pollutant**	**Ref.**
1	MoS_2 NSAs/WO_3	Photo-degradation	0.97	RhB 88.01% (5 mg L^{-1}120 min)	5
1.2	CCMs-x SVD	Photo-degradation	1.41	MB 97.85% (0.1 g L^{-1}120 min)	6
1	CS/BFs/C@MOF	Dye adsorption	1.481	MB (76.87 mg g^{-1} 420 min)	7
1	BHMS	Selective U recovery	1.39	U (5.14 ± 0.15 mg g^{-1})	8
1	g-N/WC	degradation	1.31	VOCs 99.92% (100 mg L^{-1} 30 min)	9
1	JPMS	Photo-degradation	1.49	RhB 90.1% (15 mg L^{-1}120 min)	10

1	MF-MXene/PPy	Photo-degradation	1.52	MB 92.38% (10 mg L^{-1} 240 min)	[11]
1	MSIS-3.0	Photo-degradation	1.56	RhB 83.7% (5 mg L^{-1}120 min)	[12]
1	HPM	Photo-degradation	1.85	RhB 96% (50 mg L^{-1}120 min)	[13]
1	pHLS@rGO-12	Photo-degradation	1.75	RhB 98.8% (5 mg L^{-1}120 min)	[13]
1	CuO nanowire	PMS degradation	1.42	MO 98.8% (20 mg L^{-1} 30 min)	[14]
1	Co-CAT	PMS degradation	2.2	TC 91.1% (25 mg L^{-1} 60 min)	[15]
1	TpPa-1@LiCl	Air water harvesting	0.34	/	[16]
1	FO-PE	continuous water treatment	0.585	/	[17]
1	MCS1	Synergistic Clean Water and Electricity Generation	2.67	/	[18]
1	**S-FeCu/CNF**	PMS degradation	1.76	MB 96% (20 mg L^{-1}50 min)	**This work**

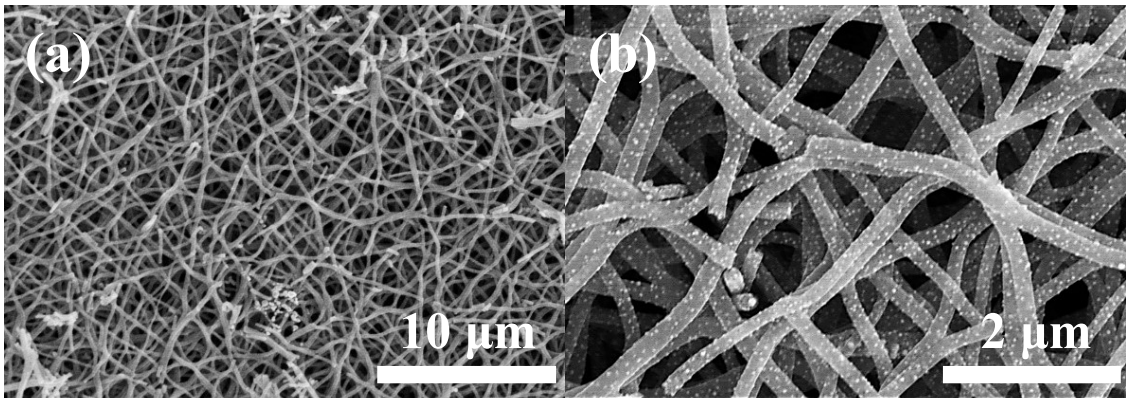

Fig. S1. (a-b) SEM images of FeCu/CNF@1 sample.

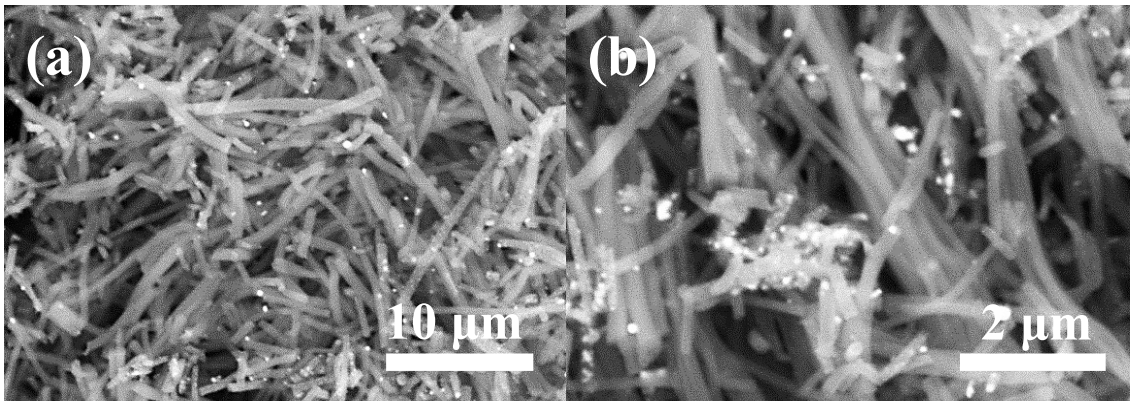

Fig. S2. (a-b) SEM images of FeCu/CNF@1.5 sample.

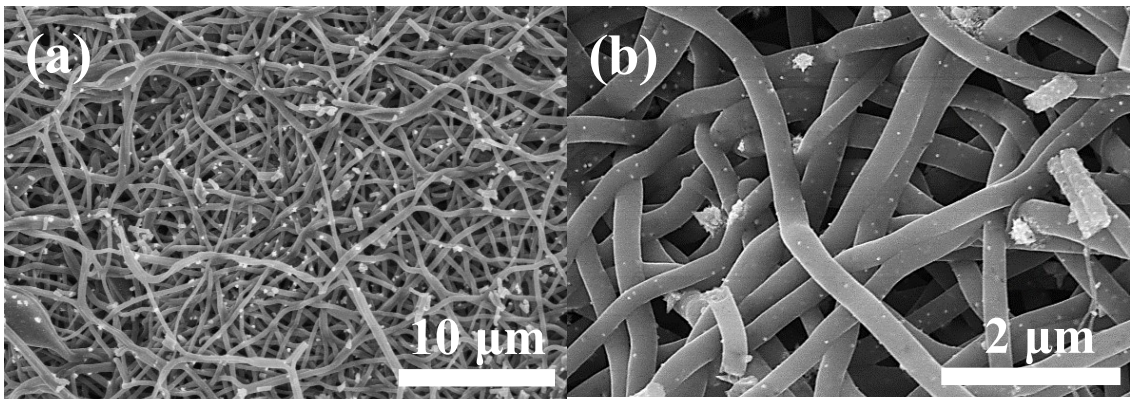

Fig. S3. (a-b) SEM images of FeCu/CNF@2 sample.

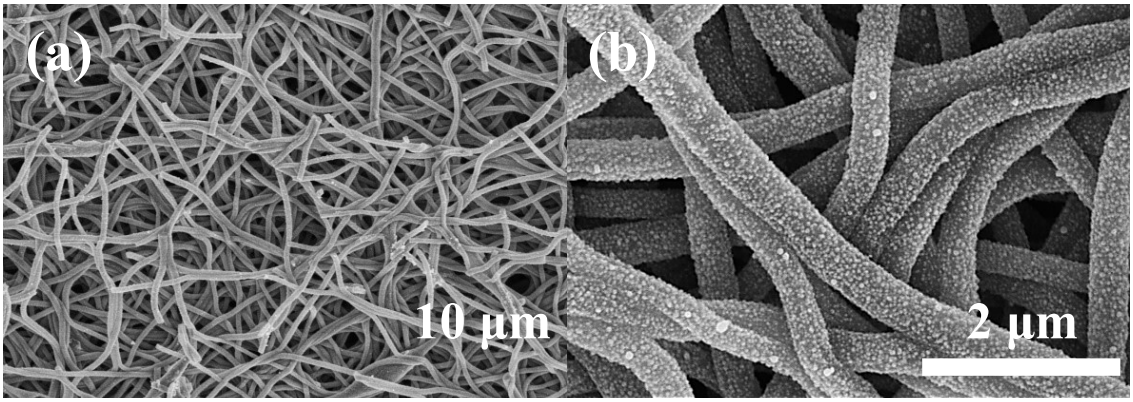

Fig. S4. (a-b) SEM images of FeCu/CNF@4 sample.

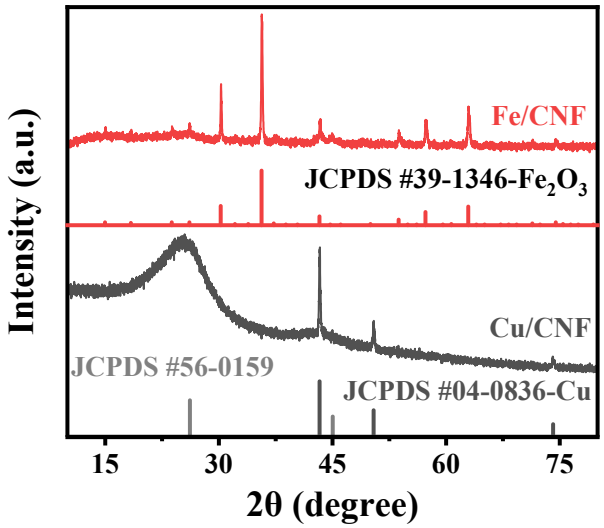

Fig. S5. XRD patterns of Fe/CNF and Cu/CNF nanocomposites.

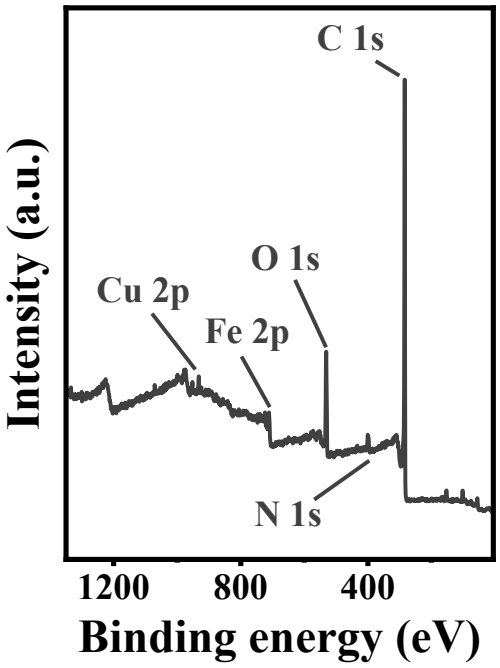

Fig. S6. XPS survey spectrum of FeCu/CNF@3 nanocomposite.

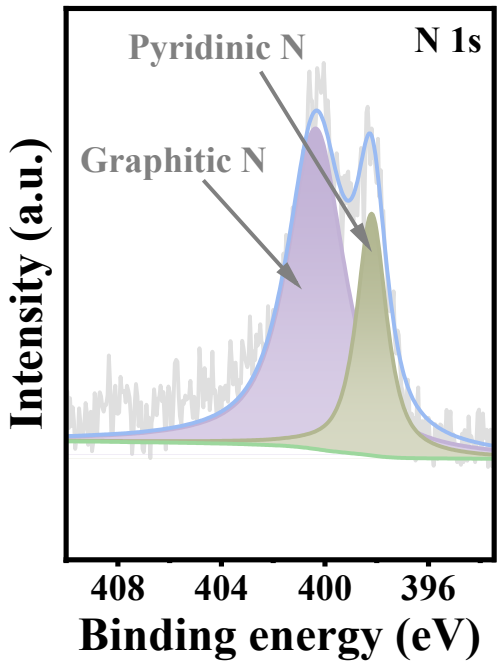

Fig. S7. High-resolution XPS N 1s spectrum of FeCu/CNF@3 nanocomposite.

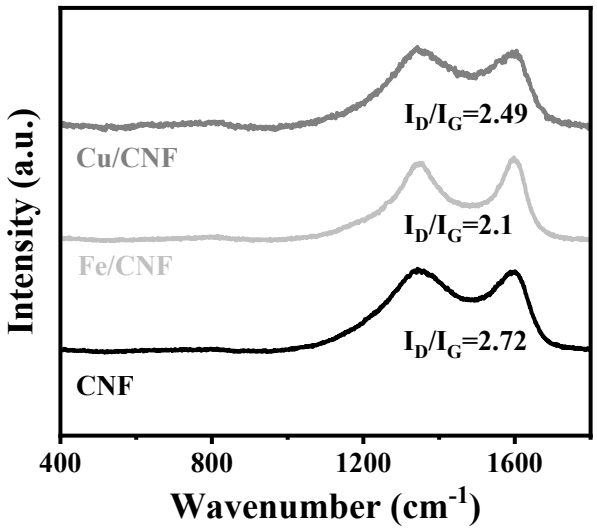

Fig. S8. Raman spectra of Fe/CNF, Cu/CNF, and CNF nanocomposites.

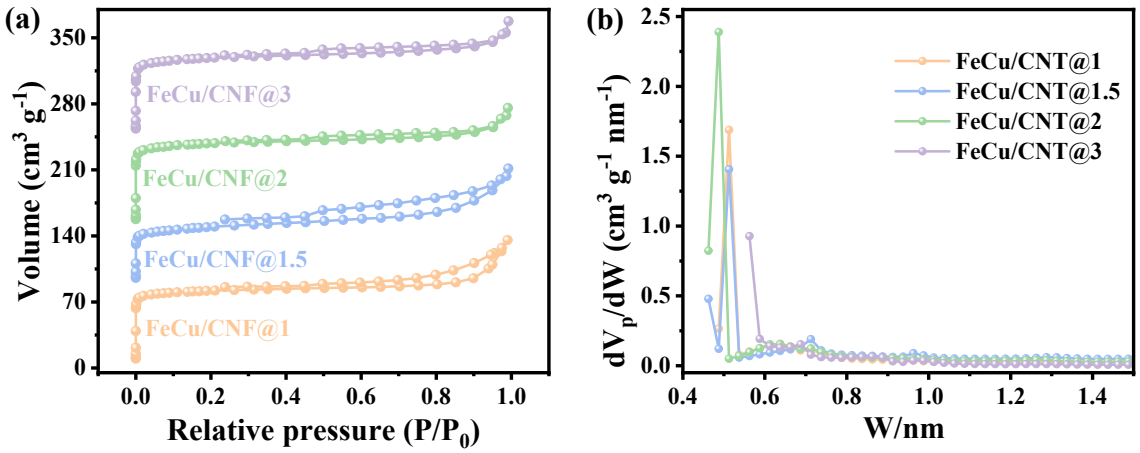

Fig. S9. (a) N2 adsorption-desorption isotherms and (b) NLDFT pore size distribution graphs of FeCu/CNF@3,2,1.5,1 nanocomposites.

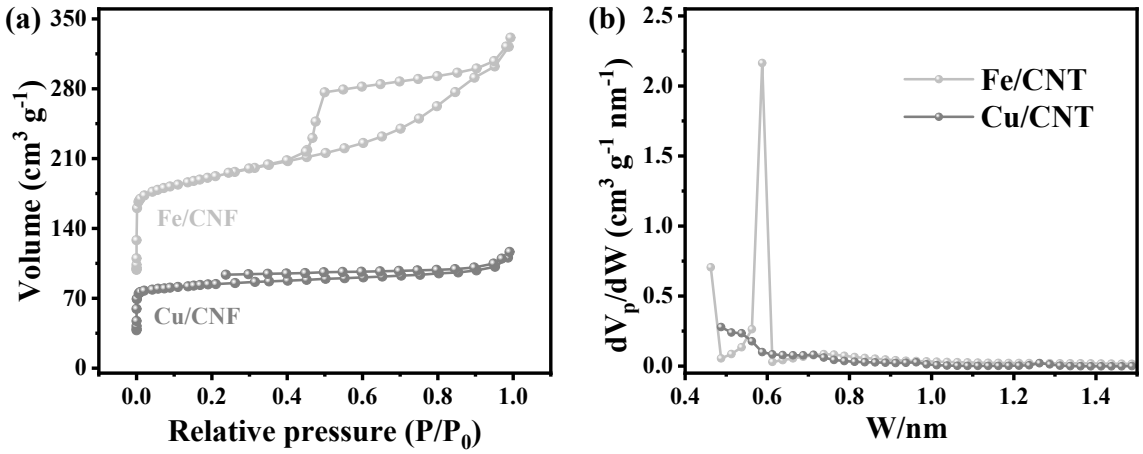

Fig. S10. (a) N2 adsorption-desorption isotherms and (b) NLDFT pore size distribution graphs of Fe/CNF and Cu/CNF nanocomposites.

Table S2. The detailed structural properties of FeCu/CNF@3, FeCu/CNF@2, FeCu/CNF@1.5, FeCu/CNF@1, Fe/CNF, and Cu/CNF nanocomposites.

Samples	S_{BET} [m^2 g^{-1}]	Total pore volume [cm^3 g^{-1}]	Average pore diameter [nm]
FeCu/CNF@1	283.52	0.20	2.75
FeCu/CNF@1.5	205.02	0.18	3.45
FeCu/CNF@2	318.09	0.18	2.28
FeCu/CNF@3	291.29	0.17	2.34
Fe/CNF	335.52	0.35	4.19
Cu/CNF	172.42	0.12	2.82

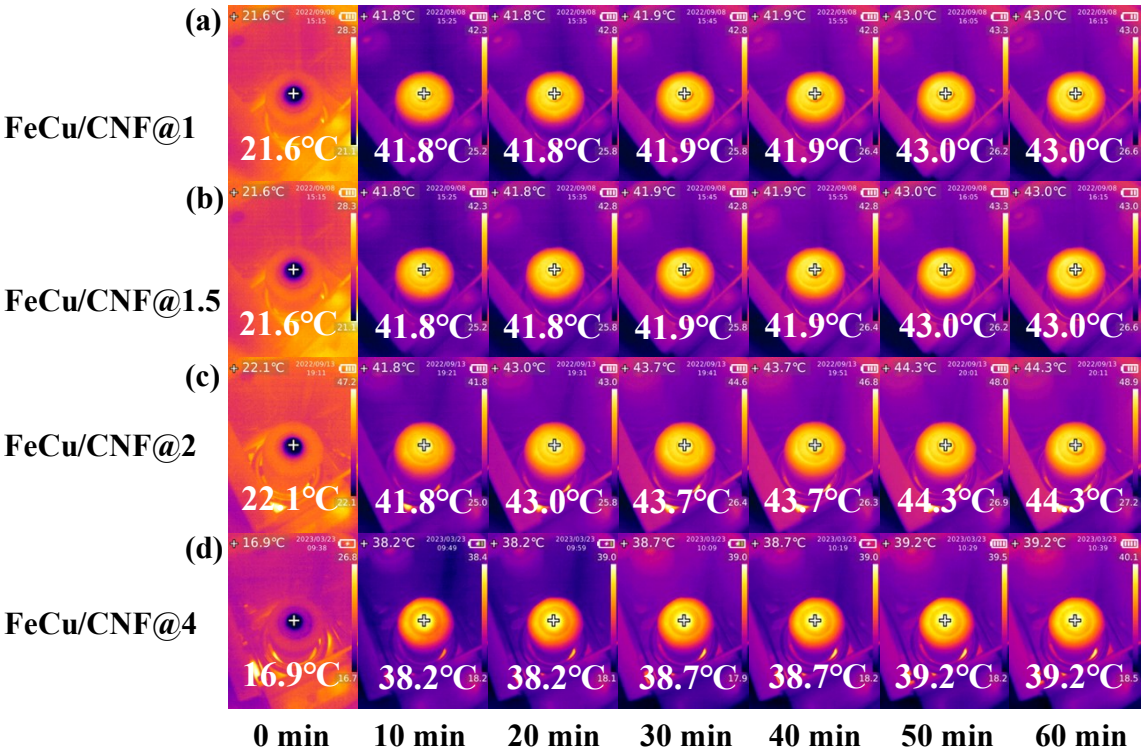

Fig. S11. Time-dependent surface temperature thermal IR images of FeCu/CNF@1 (a), FeCu/CNF@1.5 (b), FeCu/CNF@2 (c), and FeCu/CNF@4 (d) samples under one sun irradiation in air.

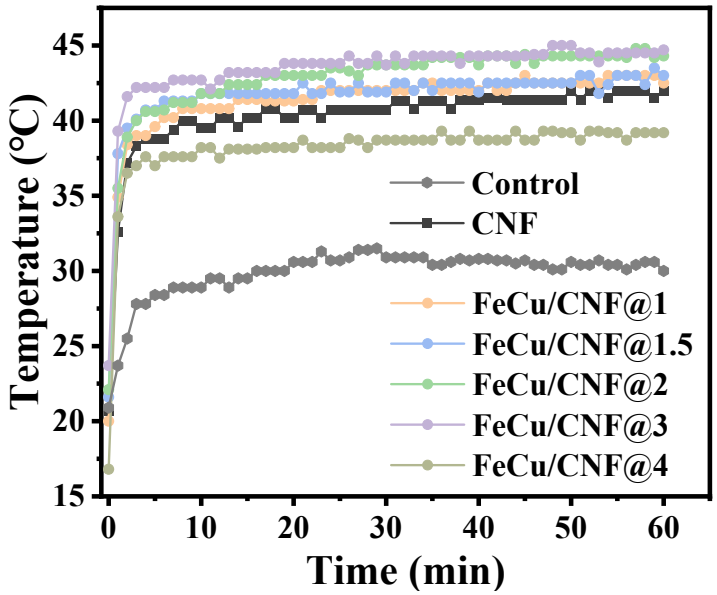

Fig. S12. Time-dependent surface temperature recordings of FeCu/CNF@1,1.5,2,3,4, CNF solar evaporator and control on water surface

under 1 sun.

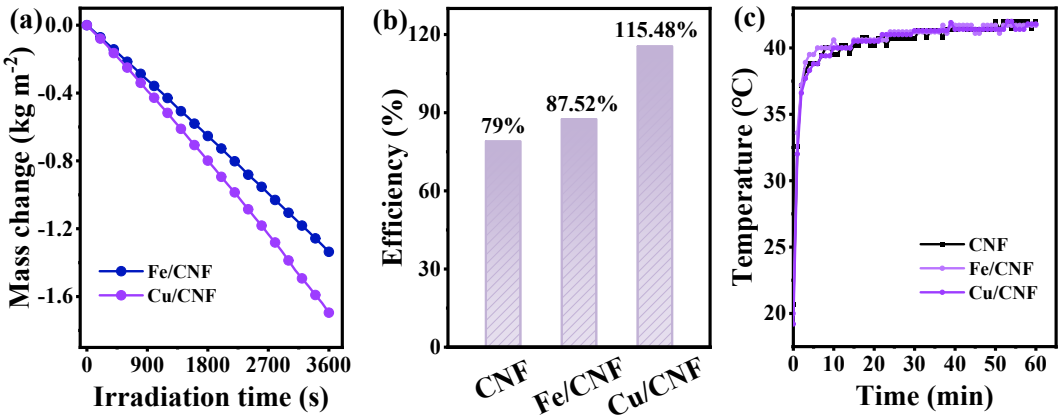

Fig. S13. (a) Cumulative mass of water as a function of time for Fe/CNF and Cu/CNF; (b) Solar evaporation efficiency performances of CNF against Fe/CNF and Cu/CNF solar evaporators; and (c) Time-dependent surface temperature recordings of Fe/CNF, Cu/CNF, and CNF solar evaporators on water surface under one sun irradiation.

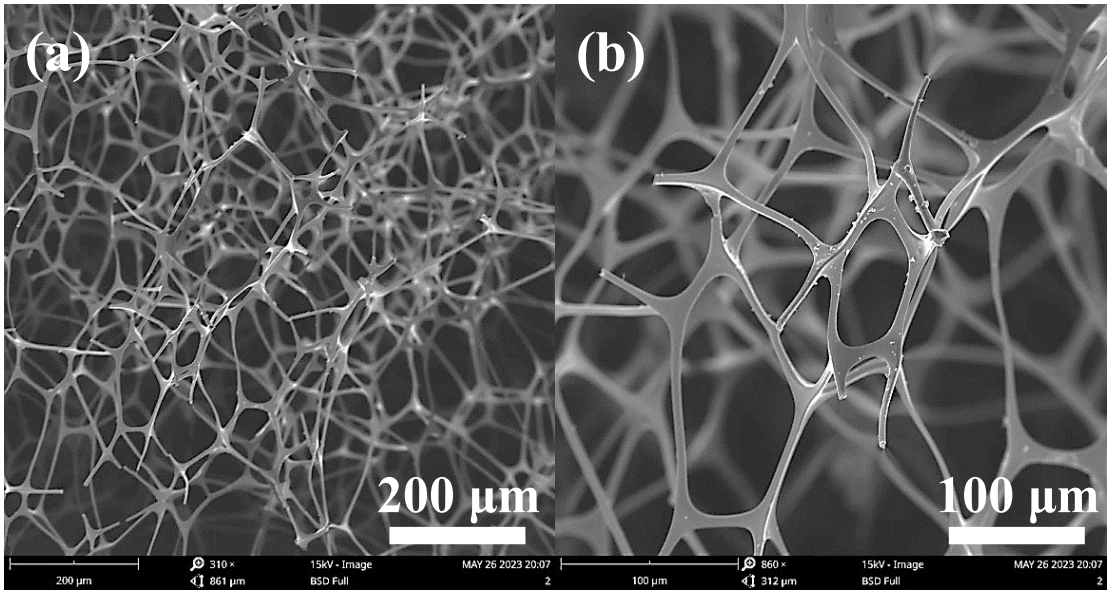

Fig. S14. (a-b) SEM images of melamine sponge skeleton.

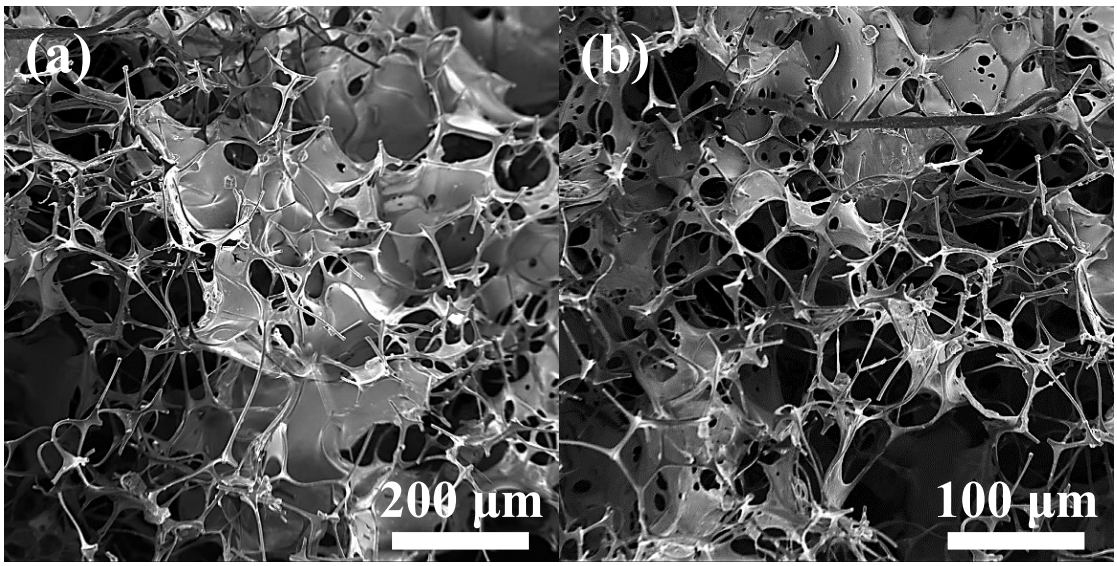

Fig. S15. (a-b) SEM images of melamine sponge skeleton coated with sodium alginate.

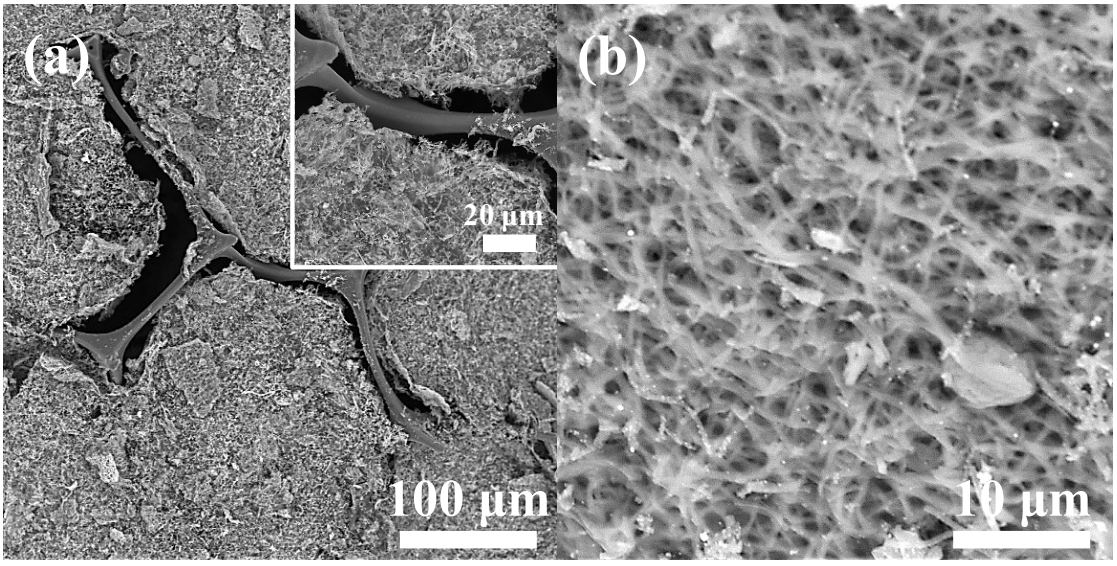

Fig. S16. (a-b) SEM images of S-FeCu/CNF sponge.

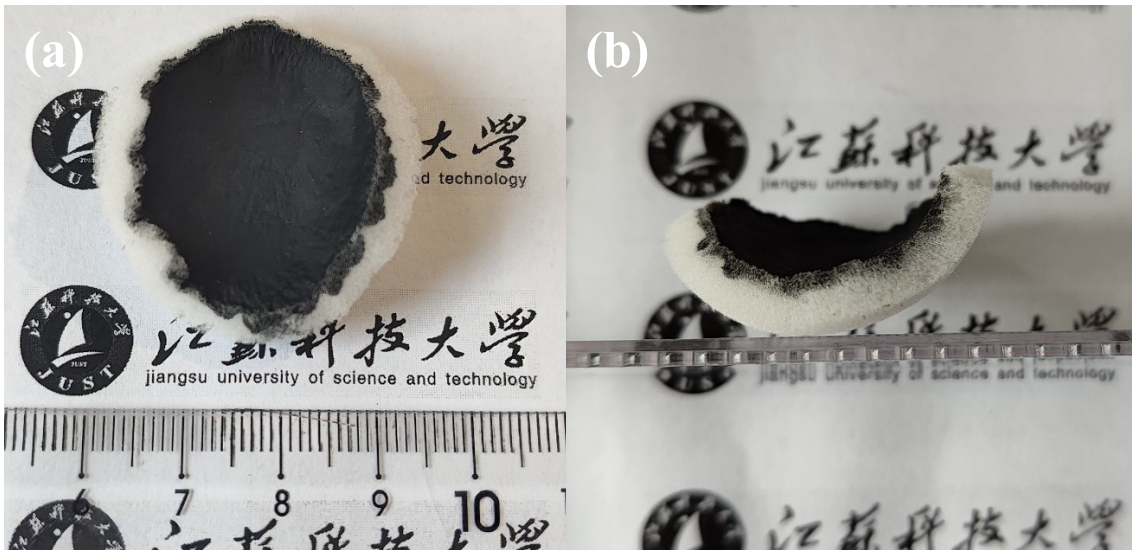

Fig. S17. (a-b) Top and side views of S-FeCu/CNF sponge with SA concentration of 4 mg mL^{-1}.

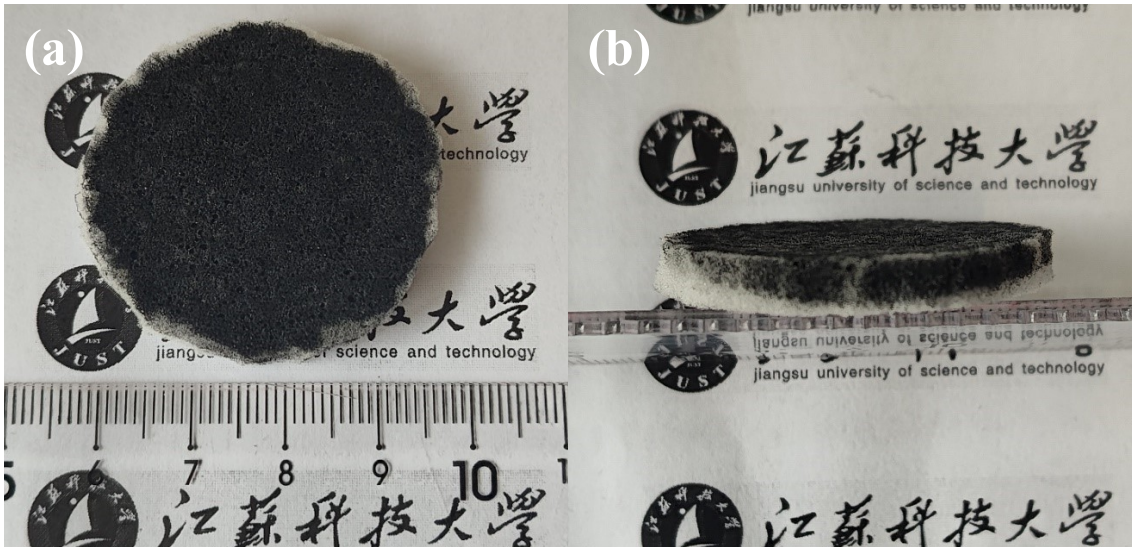

Fig. S18. (a-b) Top and side views of S-FeCu/CNF sponge with SA concentration of 1 mg mL^{-1}.

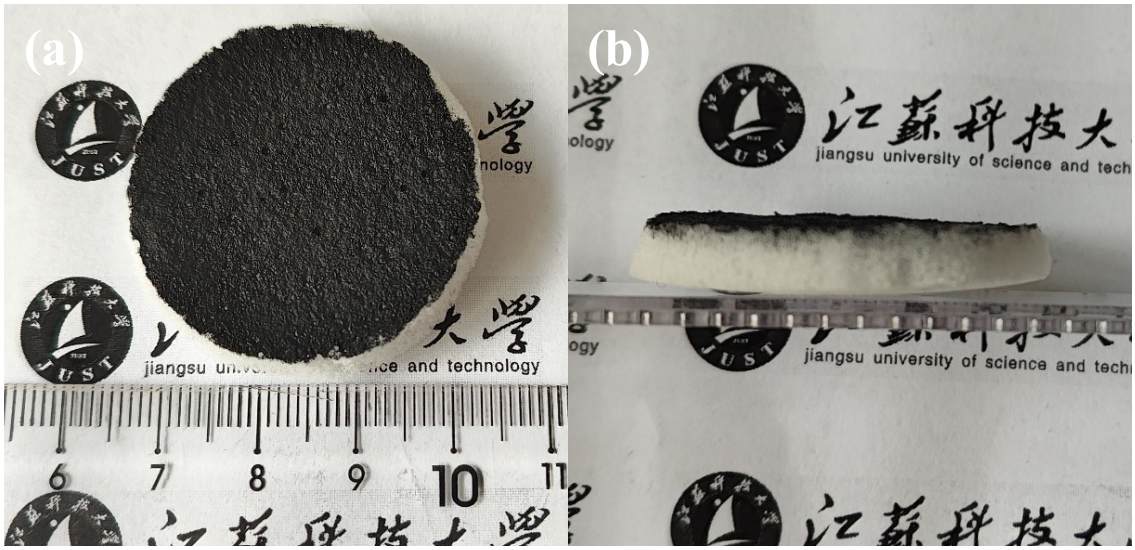

Fig. S19. (a-b) Top and side views of S-FeCu/CNF sponge with SA concentration of 2 mg mL^{-1}.

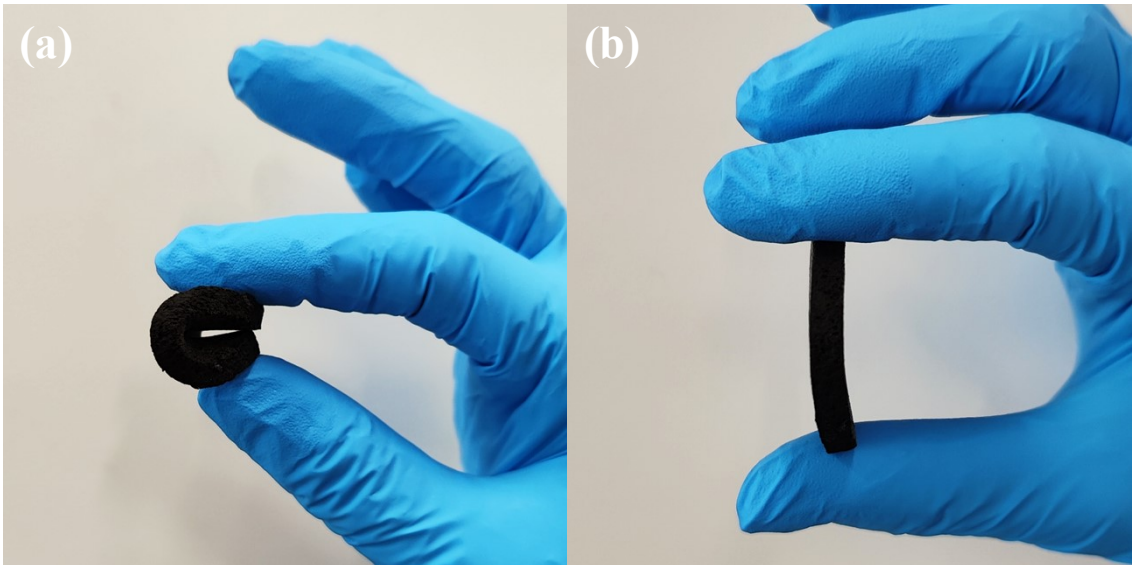

Fig. S20. (a-b) Illustration of the flexibility of dual-functional monolithic D-S-FeCu/CNF sponge evaporator (50 repeated presses).

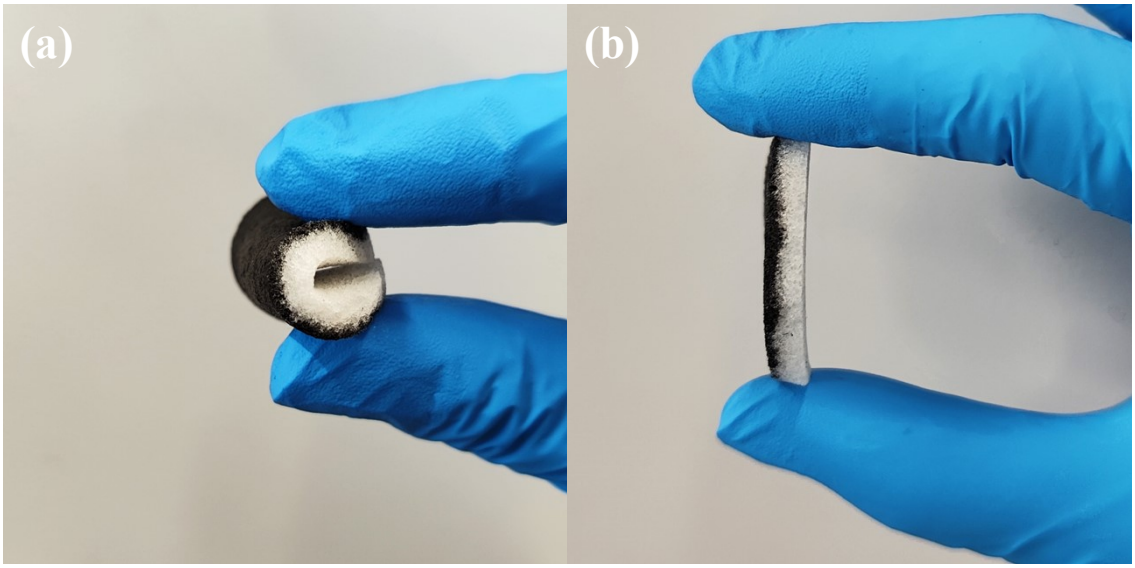

Fig. S21. (a-b) Illustration of the flexibility of S-FeCu/CNF sponge evaporator (50 repeated presses).

Fig. S22. Contact angle images of S-FeCu/CNF sponge evaporator (a), SA-coated sponge (b), and melamine sponge (c).

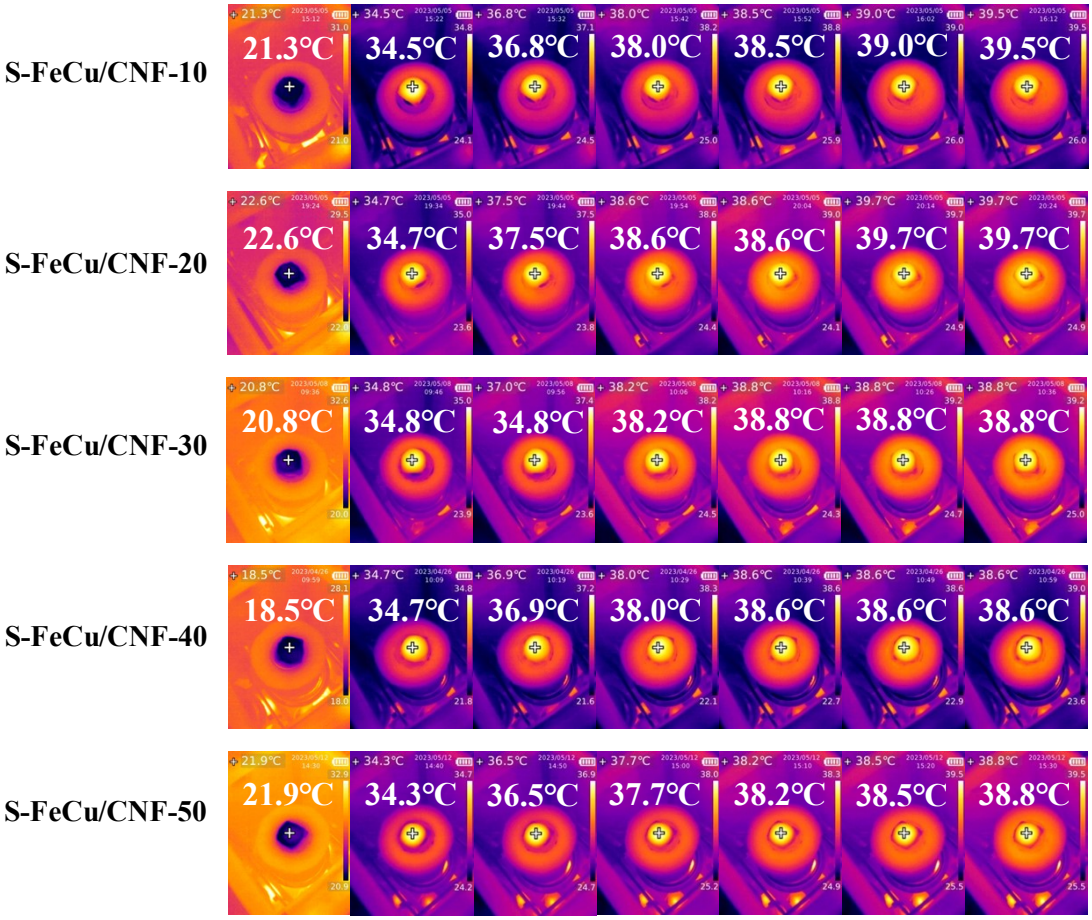

Fig. S23. IR digital images of evaporating surfaces of evaporators with different photothermal material loads in the evaporating state.

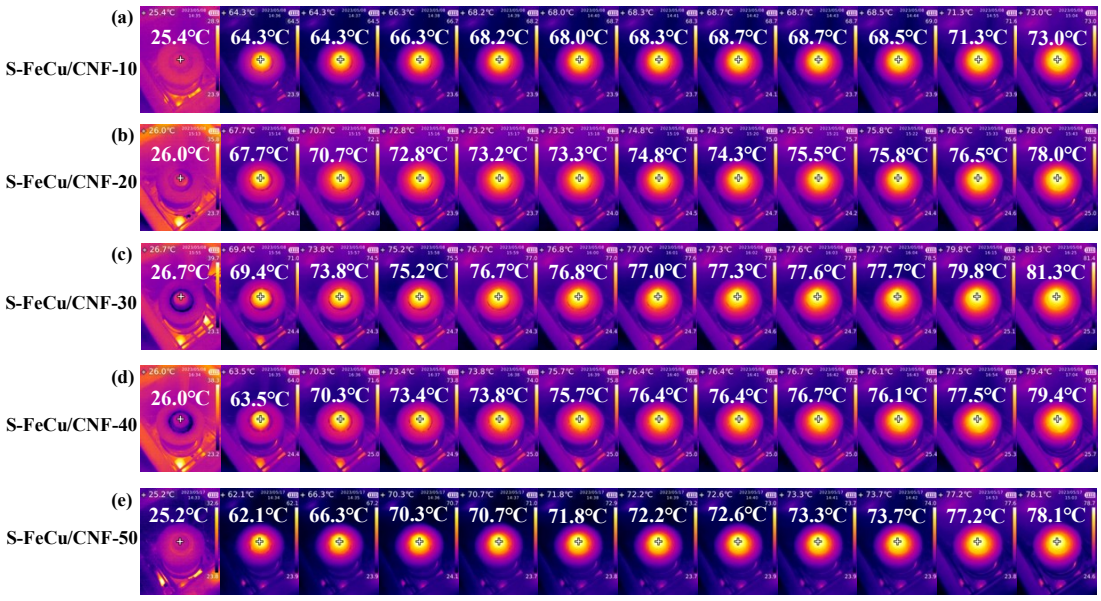

Fig. S24. IR digital images of the evaporators with different photothermal

material loads in the dried state.

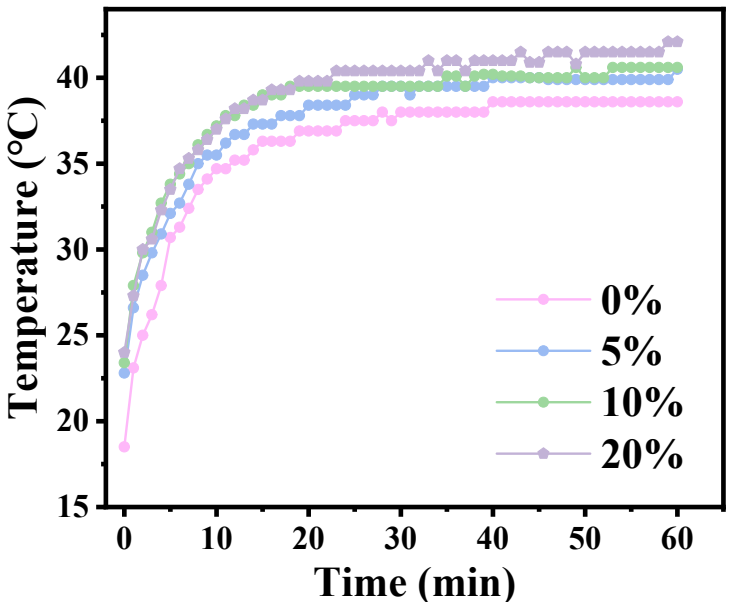

Fig. S25. Recordings of the surface temperature of an S-FeCu/CNF-40 evaporator with different salt concentrations over time under 1 sun.

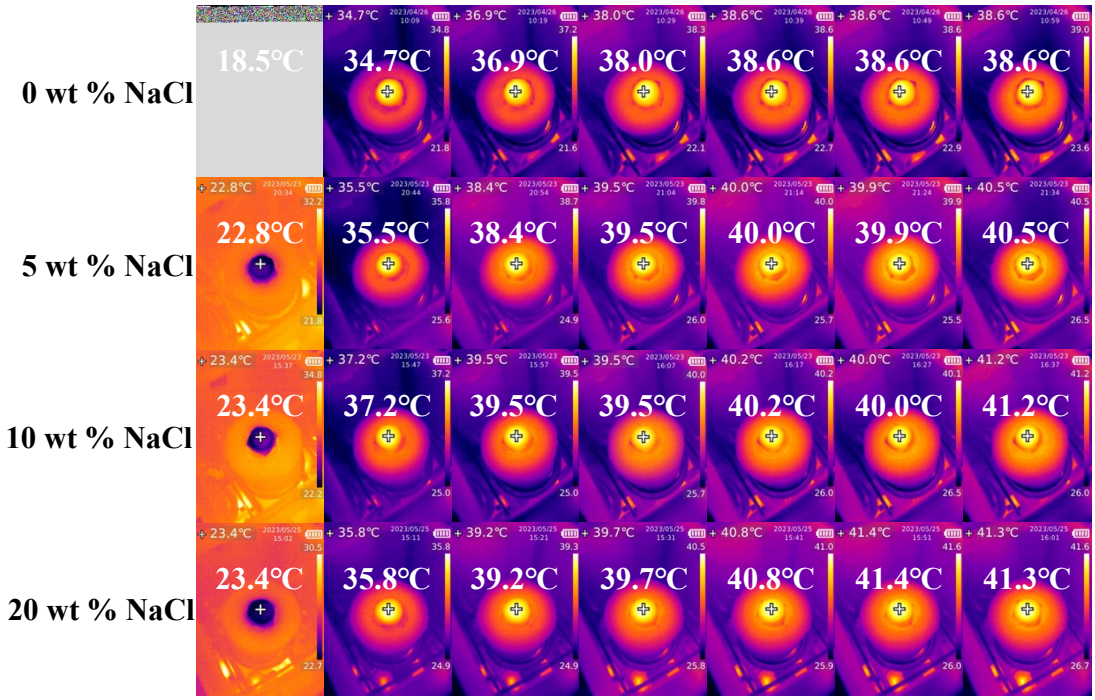

Fig. S26. IR camera evaporation surface images of S-FeCu/CNF-40 evaporator with different salt concentrations under 1 sun.

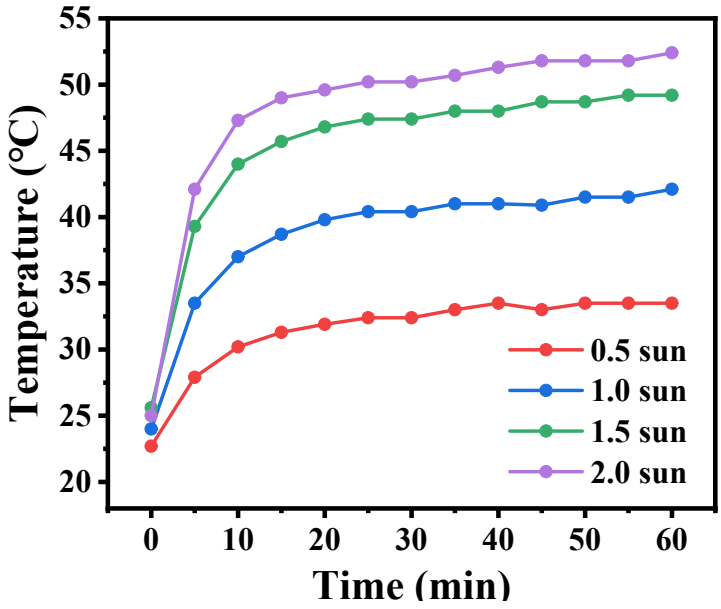

Fig. S27. Recordings of S-FeCu/CNF-40 evaporator surface temperatures with time for different solar illuminations in 20% NaCl salt solution.

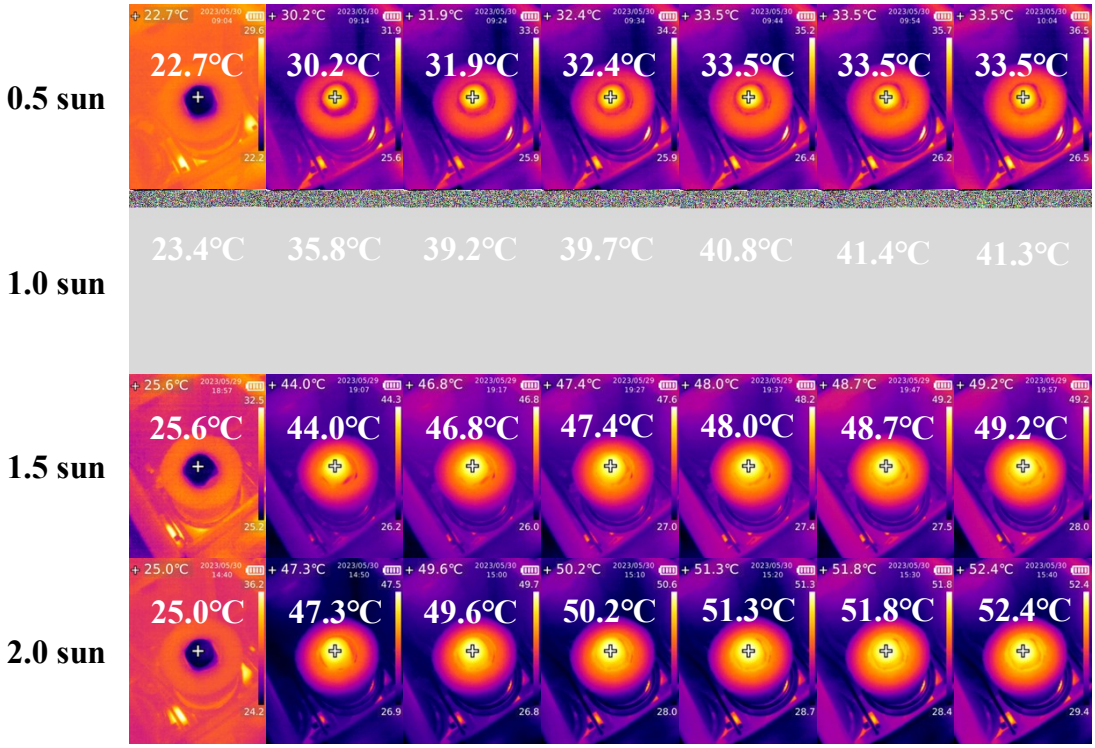

Fig. S28. IR digital images of the evaporation surface of the S-FeCu/CNF-40 evaporator under different solar illumination in 20% NaCl salt solution.

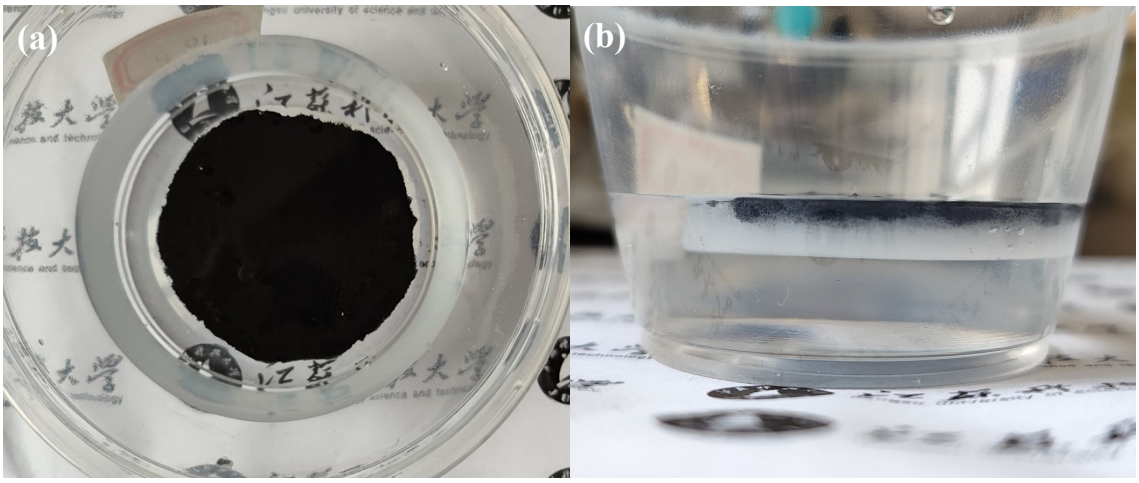

Fig. S29. (a-b) S-FeCu/CNF-40 evaporator immersed in 20 wt% NaCl solution for 6 months.

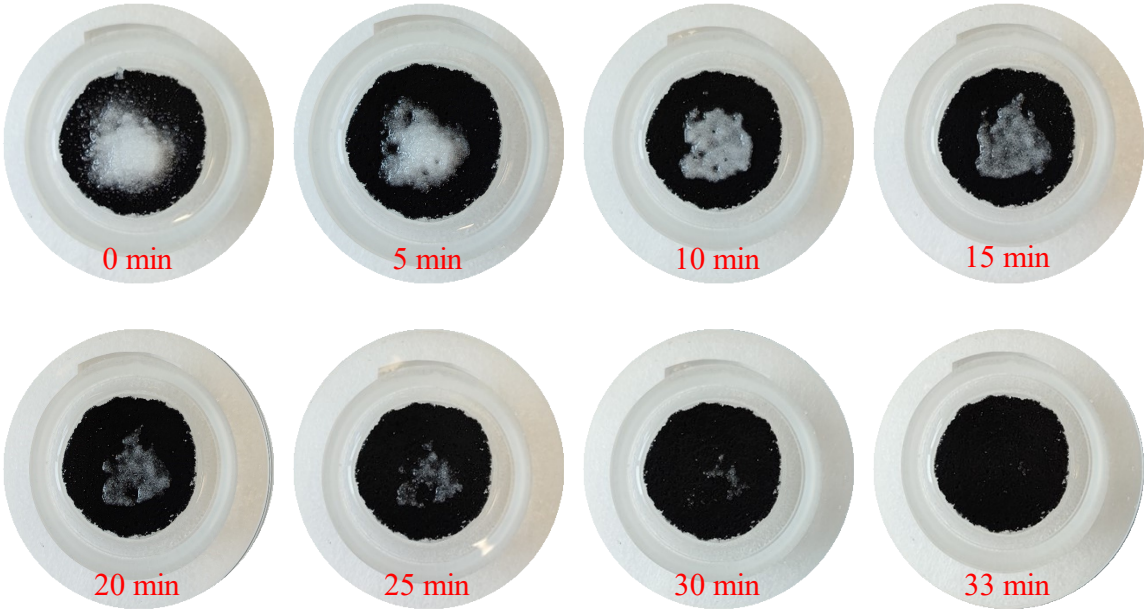

Fig. S30. (a-b) Rapid salt melt test by pouring 1 g NaCl directly onto the surface of the S-FeCu/CNF-40 evaporator.

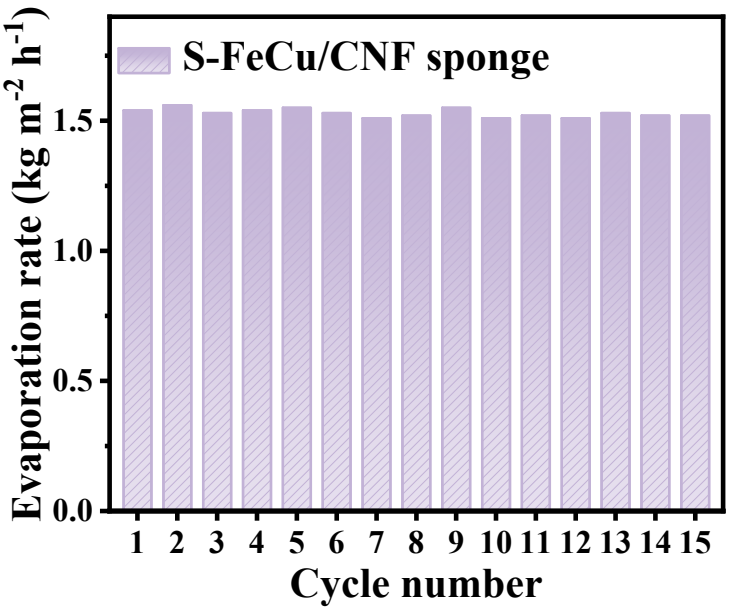

Fig. S31. Evaporation rate of S-FeCu/CNF-40 evaporator in 20 wt.% NaCl solution for 15 cycles.

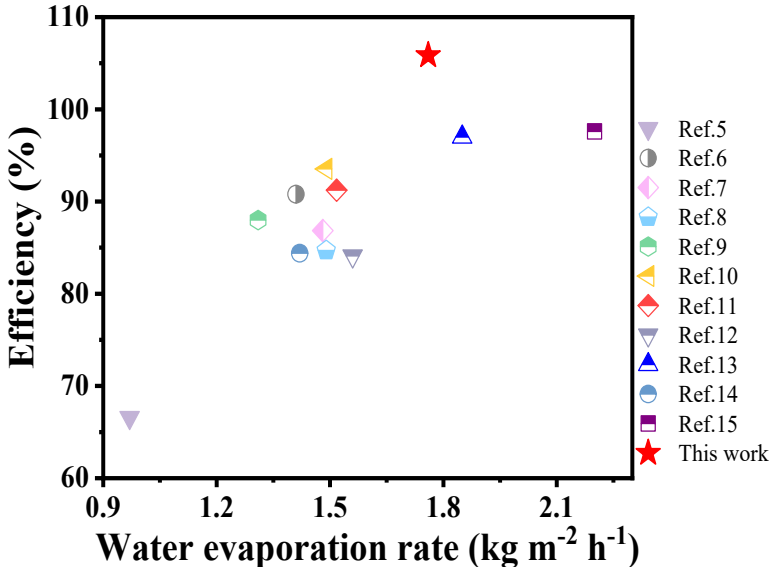

Fig. S32. Comparison of steam generation performance of S-FeCu/CNF solar evaporators with other advanced dual-function solar evaporators (**Table S1**).

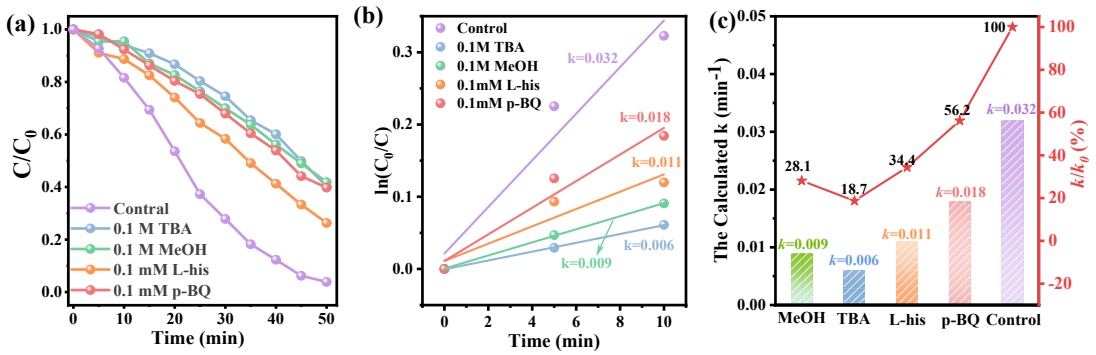

Fig. S33. (a) Quenching degradation experiment of S-FeCu/CNF; (b) corresponding fitting kinetic curves: $\ln(C_0/C)$ vs. reaction time; reaction conditions: [MB] = 20 mg L^{-1}, [PMS] = 0.049 mM, Temperature = 25 °C; (c) reaction rate constant and relationship of catalytic systems of S-FeCu/CNF involving addition of various quenching agents.

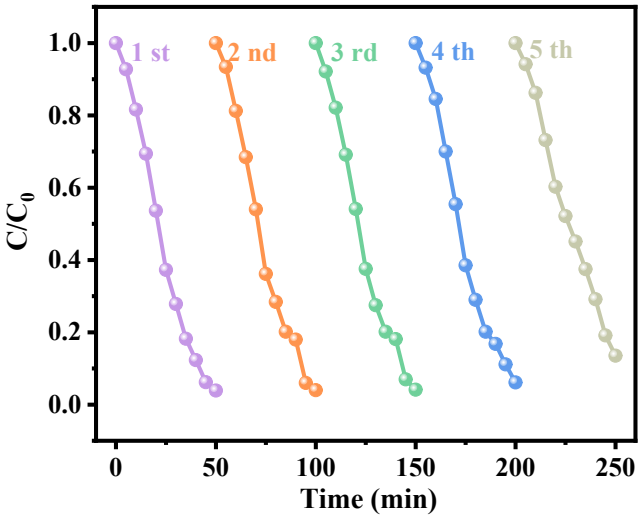

Fig. S34. The cycling experiment results of S-FeCu/CNF in activation of PMS for NFX degradation; reaction condition: [MB] = 20 mg L^{-1}, [PMS] = 0.049 mM, Temperature = 25 °C.

References:

1. M. Gao, L. Zhu, C. K. Peh and G. W. Ho, *Energy & Environ. Sci.*, 2019, 12, 841-864.
2. H. Ghasemi, G. Ni, A. M. Marconnet, J. Loomis, S. Yerci, N. Miljkovic and G. Chen, *Nat. Commun.*, 2014, 5, 4449.
3. C. Song, L. Hao, B. Zhang, Z. Dong, Q. Tang, J. Min, Q. Zhao, R. Niu, J. Gong and T. Tang, *Sci. China. Mater.*, 2020, 63, 779-793.
4. L. Zhu, M. Gao, C. K. N. Peh and G. W. Ho, *Mater. Horizons*, 2018, 5, 323-343.
5. M. Guo, B. Yuan, Y. Sui, Y. Xiao, J. Dong, L. Yang, L. Bai, H. Yang, D. Wei, W. Wang and H. Chen, *J. Colloid. Inter. Sci.*, 2023, 631, 33-43.
6. J. Wang, M. Sun, C. Liu, Y. Ye, M. Chen, Z. Zhao, Y. Zhang, X. Wu, K. Wang and Y. Zhou, *Adv. Mater.*, 2023, 35, 2306103.
7. X. Sun, X. Jia, H. Weng, J. Yang, S. Wang, Y. Li, D. Shao, L. Feng and H. Song, *Sep. Purif. Technol*, 2022, 301, 122010.
8. W.-R. Cui, C.-R. Zhang, R.-P. Liang, J. Liu and J.-D. Qiu, *ACS Appl. Mater. & Inter.*, 2021, 13, 31561-31568.
9. Z. Yang, L. Chen, Y. Chen, Y. Ju, Z. Zhang, Z. Zhang, Z. Wang, C. Chen, X. Lu, C. Chen and F. Chen, *Desalination*, 2023, 555, 116536.
10. L. Zhang, X. Wang, X. Xu, J. Yang, J. Xiao, B. Bai and Q. Wang, *Sep. Purif. Technol*, 2022, 298, 121643.
11. X. Mu, L. Chen, N. Qu, J. Yu, X. Jiang, C. Xiao, X. Luo and Q. Hasi, *J.*

Colloid. Inter. Sci., 2023, 636, 291-304.

12. B. Yuan, Y. Sui, J. Dong, X. Lv, M. Guo, Y. Xiao, L. Yang, H. Yang, L. Bai, W. Wang, D. Wei, Y. Liang and H. Chen, *Appl. Sur. Sci.*, 2023, 611, 155678.
13. J. Wu, J. Qu, G. Yin, T. Zhang, H.-Y. Zhao, F.-Z. Jiao, J. Liu, X. Li and Z.-Z. Yu, *J. Colloid. Inter. Sci.*, 2023, 637, 477-488.
14. Y. Xu, J. Ma, Y. Han, J. Zhang, F. Cui, Y. Zhao, X. Li and W. Wang,*ACS Sustain. Chem. & Eng.*, 2019, 7, 5476-5485.
15. P. He, H. Lan, H. Bai, Y. Zhu, Z. Fan, J. Liu, L. Liu, R. Niu, Z. Dong and J. Gong, *Appl. Catal. B: Environ.*, 2023, 337, 123001.
16. Y. Wang, W. Chen, J. Fu and Y. Liu, *eScience*, 2023, 3, 100154.
17. X. Song, W. Dong, Y. Zhang, H. M. Abdel-Ghafar, A. Toghan and H. Jiang, *Exploration*, 2022, 2, 20220054.
18. R. Niu, J. Ren, J. J. Koh, L. Chen, J. Gong, J. Qu, X. Xu, J. Azadmanjiri and J. Min, *Adv. Ener. Mater.*, 2023, 13, 2302451.